Journal of Power Sources 272 (2014) 398–403

Contents lists available at ScienceDirect

Journal of Power Sources

journal homepage: www.elsevier.com/locate/jpowsour

The role of FeS in initial activation and performance degradation of Na–$NiCl_2$ batteries

Guosheng Li [a], Xiaochuan Lu [a], Jin Y. Kim [a, *], Mark H. Engelhard [b], John P. Lemmon [a], Vincent L. Sprenkle [a]

[a] Energy Processes & Materials Division, Pacific Northwest National Laboratory, Richland, WA 99352, USA
[b] Environmental and Molecular Sciences Laboratory, Pacific Northwest National Laboratory, Richland, WA 99352, USA

HIGHLIGHTS

- FeS plays a critical role in initial activation of Na–$NiCl_2$ battery.
- The formation of polysulfide is related to the removal of the passivation layer.
- There is an optimum level of FeS that minimizes degradation of cells.

ARTICLE INFO

Article history:
Received 13 June 2014
Received in revised form
21 August 2014
Accepted 25 August 2014
Available online 2 September 2014

Keywords:
Sodium-nickel chloride battery
Cell activation
Ni particle growth
Passivation layer
Cathode additives

ABSTRACT

The role of iron sulfide (FeS) in initial cell activation and degradation in Na–$NiCl_2$ battery was investigated in this work. The research focused on identifying the effects of FeS levels on the electrochemical performance and morphological changes in the cathode. The x-ray photoelectron spectroscopy study along with battery tests revealed that FeS plays a critical role in initial battery activation by removing passivation layers on Ni particles. It was also found that the optimum level of FeS in the cathode resulted in suppressing Ni particle growth and improved battery cycling performance. The results of electrochemical characterization indicated that sulfur species generated *in situ* during initial charging, such as polysulfide and element sulfur, are responsible for removing the passivation layer. Consequently, the cells containing elemental sulfur in the cathode exhibited similar electrochemical behavior during initial charging compared to the cells containing FeS.

Published by Elsevier B.V.

1. Introduction

Molten-sodium-based batteries have been investigated for a couple of decades, since Kummer and Weber of the Ford Motor company proposed a sodium–sulfur (Na–S) battery for a train development program in 1967 [1,2]. Although molten-sodium-based batteries were initially developed for transportation applications, molten-sodium-based batteries such as Na–S and sodium-metal halide (ZEBRA) batteries are now recognized as one of the most promising candidates for large-scale energy storage systems for renewable energy and grid applications [3–7]. Na–S batteries and ZEBRA batteries share common features, such as a molten sodium anode and β″ alumina solid electrolyte (BASE) in the cell architecture. In the case of the ZEBRA battery, the use of solid metal halides ($NiCl_2$, $FeCl_2$, etc.) as active cathode ingredients requires a molten secondary electrolyte, sodium tetrachloroaluminate ($NaAlCl_4$), in order to facilitate movement of the Na^+ ion in the cathode [8–12]. The ZEBRA battery provides several benefits over the Na–S battery, including high open-circuit voltage, lower operating temperature, safe cell-failure mode, and ease of assembly in the discharged state without using metallic sodium in the anode [3,5,7].

Among ZEBRA batteries, the sodium–nickel chloride (Na–$NiCl_2$) battery has been most widely investigated as a promising system for application to large-scale energy storage [13]. A tubular Na–$NiCl_2$ battery is operated in the temperature range between 250 and 300 °C in order to achieve adequate ionic conductivity of the solid electrolyte and secondary liquid electrolyte [14]. Electrochemical reactions of a Na–$NiCl_2$ battery during charging and discharging processes are described as follows: [14]

Charge state ↔ Discharge state:

Na (molten) ↔ $Na^+ + e^-$ anode reaction

* Corresponding author. Tel.: +1 509 375 2225; fax: +1 509 375 2186.
E-mail addresses: Jin.Kim@pnnl.gov, jinykim8z@gmail.com (J.Y. Kim).

http://dx.doi.org/10.1016/j.jpowsour.2014.08.106
0378-7753/Published by Elsevier B.V.

$NiCl_2 + 2Na^+ + 2e^- \leftrightarrow Ni + 2NaCl$ cathode reaction

Overall redox reaction:

$$2Na + NiCl_2 \leftrightarrow 2NaCl + Ni,\ E_0 = 2.58\ V \text{ at } 300\ ^\circ C \quad (1)$$

Unlike a Na–S battery, a Na–$NiCl_2$ battery is typically assembled in the discharged state, avoiding the use of reactive, hazardous materials such as anhydrous nickel chloride and metallic sodium [15]. The starting cathode materials in the discharged state consist of fine nickel powder, sodium chloride powder, and a few other ingredients as additives [14,16]. During the initial charging process, Ni is oxidized to form $NiCl_2$ in the cathode and Na ions from NaCl are reduced to metallic Na in the anode after transporting through the BASE. The key feature of a Na–$NiCl_2$ battery is the charging step, which is considered the rate limiting step due to the formation of a poorly conductive $NiCl_2$ layer on the surfaces of Ni particles and the sluggish dissolution of NaCl particles in the melts ($NaAlCl_4$) [16]. The active surface area of Ni particles, which relates to Ni particle size and Ni content (NaCl/Ni ratio), is one of the critical factors for battery performance because the Ni redox reaction can only occur on the surfaces of electrically conducting Ni particles [16–18]. Among additives blended in the cathode materials, such as other sodium halides (NaF, NaI), aluminum powder, and iron sulfide (FeS), FeS is considered the most important additive for the Na–$NiCl_2$ battery [14]. However, despite the importance of using FeS in the Na–$NiCl_2$ battery, only limited experimental results are available to understand its role. To our best knowledge, the detailed electrochemical reaction mechanisms of FeS in the Na–$NiCl_2$ battery have not yet been clearly identified.

In this work, extensive investigations were performed to understand the role of FeS additives in the Na–$NiCl_2$ battery. X-ray photoelectron spectroscopy (XPS) was conducted to identify the reactions of FeS on the Ni surfaces. The morphological changes of Ni particles were also closely monitored with different levels of FeS in the cathode. Based on the results of electrochemical tests, XPS and scanning electron microscopy, the roles of FeS in the cathode will be discussed, including the removal of passivation layers on the Ni particles.

2. Experimental

2.1. Material preparation

Cathode materials used in this work consisted of Ni (Novamet, Type 255), NaCl (Alfa Aesar, 99.99%), and additives (FeS, aluminum, NaI, and NaF) reported in our previous publications [10]. The amounts of FeS loadings were 0.01, 0.1, 1 and 2 mol% in the cathode mixture, which were referred to as 0.01×, 0.1×, 1×, and 2×, respectively. For comparison, cells with 1× elemental sulfur (Sigma Aldrich, 99.5%) loading (1 mol% elemental sulfur) were prepared. The cathode materials were thoroughly mixed using a low-energy ball milling method followed by the formation of granules using a granulator (Freund TF-Labo). The $NaAlCl_4$ secondary electrolyte was prepared using the procedure reported in our previous publications [19]. ~1 g of cathode granules with the Ni/NaCl molar ratio of 1.82 was used in each cell, corresponding to a theoretical capacity of 157 mAh.

2.2. Planar button cell and cell tests

The button cell consisted of the battery case (cathode and anode cases), α-alumina (99.5% purity) fixture, and BASE (3 cm^2 active area) as reported in our previous publications [16,18].

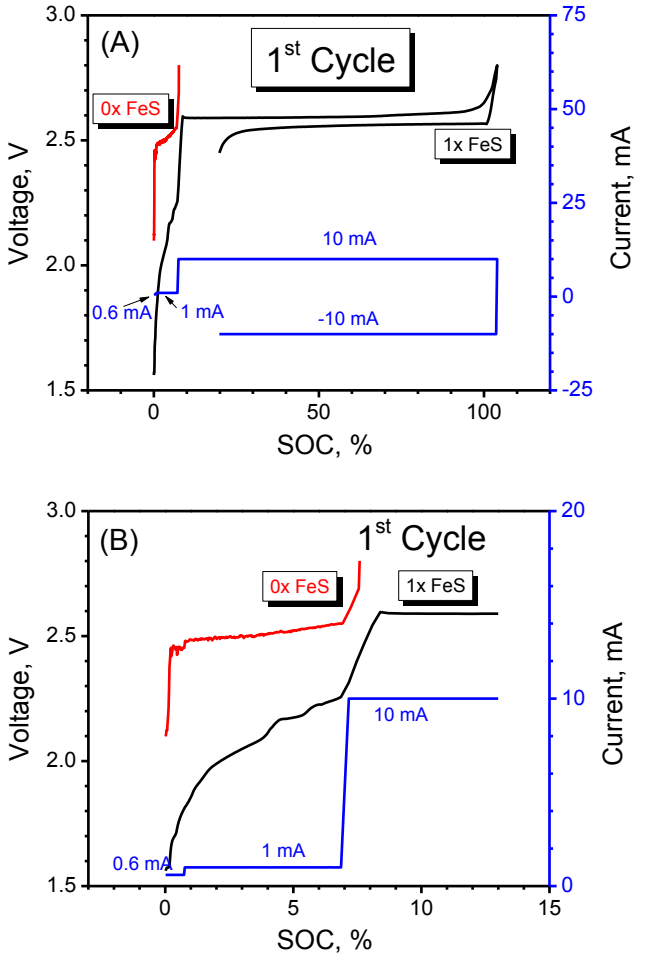

Fig. 1. (A): Voltage profiles (first cycle) for batteries with FeS (1× loading, black) and with no FeS (0× loading, red). The first charging consists of three steps: 0.6 mA (2 h), 1 mA (10 h), and 10 mA (cutoff at 2.8 V). The discharge step is a constant current discharge at −10 mA (capacity cut at 20% SOC). (B): Expanded view of voltage profiles of first charge in low-current charging periods for cells with 0× (red) and 1× FeS (black) in the cathode. (For interpretation of the references to color in this figure legend, the reader is referred to the web version of this article.)

Composite yttria-stabilized zirconia (YSZ)/β″ alumina BASE discs were fabricated using the vapor phase conversion process [20]. The thickness of the BASE disc after conversion and creep-flattening was 500 μm. Before loading any active materials, a BASE disc was glass-sealed to an α-alumina fixture. The anode side of a BASE disc was further treated with an aqueous lead acetate ($Pb[CH_3COO]_2$) solution and heat treated at 400 °C under nitrogen in order to improve the wettability of the molten sodium [16].

Cell tests were carried out using an Arbin potentiostat (MSTAT 8000) controlled by vendor supplied software (MITS Pro). The maiden (first) charging process of the cells was conducted following three steps with different charging currents (0.6 mA for 2 h, 1 mA for 10 h, and 10 mA until the cell voltage reached 2.8 V) until the full capacity was achieved. For the maiden discharge, the cells were discharged at a constant current (10 mA, C/15) until the state of charge (SOC) of cells reached 20% (30 mAh). Once the maiden charge and discharge processes were completed, the cells were cycled with a fixed cycling capacity window (30–120 mAh) at C/3 (30 mA) with respect to the cycling capacity (90 mAh).

2.3. Characterization

After battery tests, the fracture surfaces of the cathodes were observed using a scanning electron microscope (SEM, JEOL JSM-5900LV) equipped with an Oxford energy dispersive x-ray spectrometry (EDS) system. The particle sizes of Ni in the cathodes were measured from SEM micrographs and elemental mappings of Ni.

XPS was performed on raw Ni powder and a partially charged cathode using a Physical Electronics Quantum 2000 Scanning ESCA Microprobe equipped with a 16 element multichannel detector. This system uses a focused monochromatic Al Kα x-ray (1486.7 eV) source and a spherical section analyzer. The partially charged cathode (marked as "Cathode" in Fig. 2) was prepared by charging the cell with 1X FeS up to the end of the second step (~7% SOC) during the maiden charge. Melts ($NaAlCl_4$) in the cathode sample were washed out with tetrahydrofuran (THF) in a nitrogen-purged glove box to analyze the surfaces of Ni particles.

3. Results and discussion

Fig. 1 shows the first-cycle charge–discharge curves of cells with no FeS (0×) and 1× FeS. The cell containing 1× FeS revealed a gradual voltage increase during the low-current charging steps (0.6 mA and 1 mA). The initial voltage of the cell containing 1× FeS started from ~1.6 V, indicating the oxidation of aluminum additive in the cathode (Al/Al^{3+} redox potential: 1.58 V with respect to Na/Na^{+}). There was a slow voltage rise from 1.6 to 2.2 V during the lower-current charging steps (≤1 mA). The cell voltage climbed up to a plateau around 2.6 V during the third charging step at 10 mA, indicating the oxidation of Ni to Ni^{2+} (2.58 V with respect to Na/Na^{+}). At the end of charging, a sharp increase in the cell voltage was observed, implying a depletion of NaCl in the cathode. In contrast with the 1× FeS-loaded cell, a cell without FeS (0× FeS) exhibited a high voltage profile (~2.5 V) during the lower-current charging periods. The cell without FeS quickly reached 2.8 V at 10 mA without showing a plateau related to the Ni/Ni^{2+} reaction at ~2.6 V. Consequently, no discharge capacity was observed during discharging. This result implies that the $Na–NiCl_2$ battery using conventional Ni powder could not be charged without FeS additive in the cathode.

To understand the role of FeS in the initial activation of the $Na–NiCl_2$ battery, XPS analysis was performed on the surface of particles of raw Ni powder as well as as-charged cells with FeS. Fig. 2A and 2C show wide XPS spectra collected from raw Ni powder and cathode samples with 1× FeS after charging up to ~7% SOC, respectively. The cathode was washed with THF to remove catholyte melts and to expose the Ni surface for XPS analysis. High resolution XPS spectra related to Ni $2p_{1/2}$ and Ni $2p_{3/2}$ are shown in Fig. 2B (raw Ni powder) and 2D (charged cathode). More attention was given to Ni $2P_{3/2}$ spectra at lower binding energy because a better signal/noise ratio was observed for Ni $2P_{3/2}$ spectra comparing to Ni $2P_{1/2}$ at higher binding energy. The spectral line at 852.7 eV is assigned to metallic Ni^0 while the peak at 861.5 eV is attributed to the shake-up satellite peak of NiO as reported in the literature [21]. The peak at 855.8 eV shown in Fig. 2B is interpreted as multiple assignments including $Ni(OH)_2$, Ni_2O_3 and NiO(OH) [22]. A high resolution XPS spectrum collected from raw Ni powder clearly exhibited the presence of a passivation layer (oxide and hydroxide) on the surface of the Ni powder (Fig. 2B). The passivation layer on the surface of the Ni powder can hinder

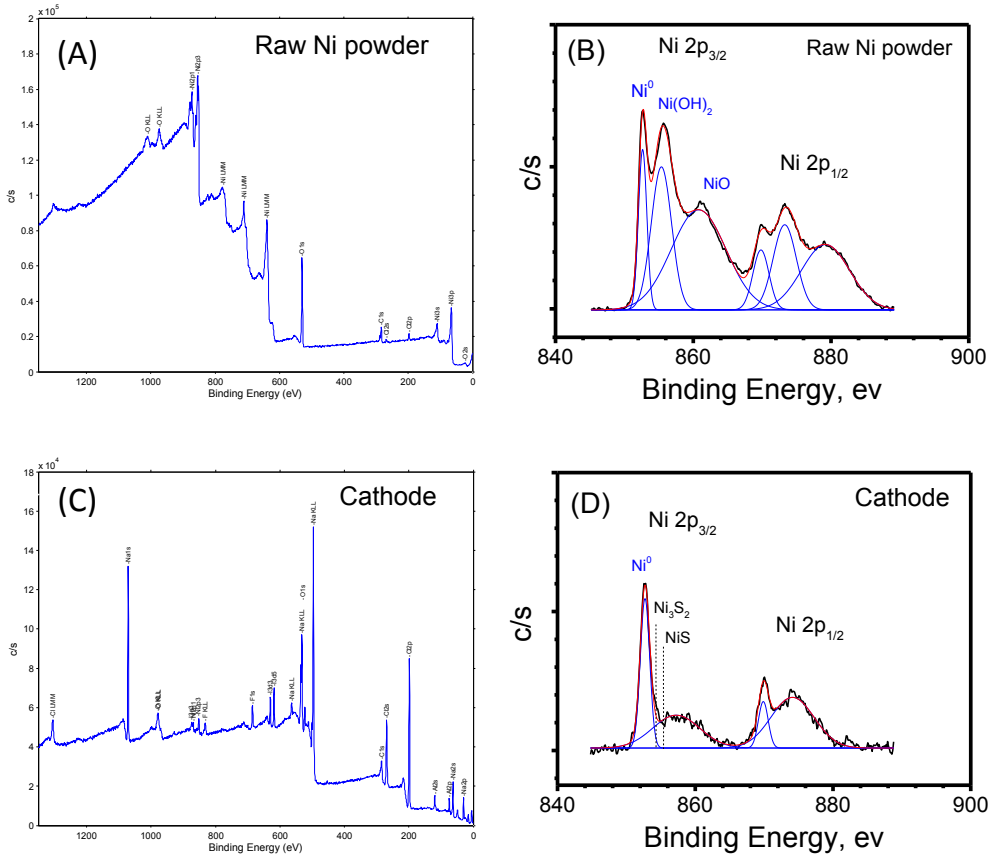

Fig. 2. Wide scan of XPS spectra for raw Ni powder (A), and cathode (C). "Cathode" refers to cathode granules taken from batteries charged up to the second step (1 mAh, 10 h) and washed with THF. See experimental section for the detailed sample preparation method. High resolution XPS spectra for raw Ni powder (B), and for cathode (D).

electrochemical reactions in the cathode due to (1) increase in ohmic resistance for the current path and (2) decrease in the electronically active surface area, as indicated by the poor electrochemical performance of cells without FeS additive shown in Fig. 1.

On the other hand, Ni $2p_{3/2}$ peaks collected from a partially charged cathode (Fig. 2D) revealed an intense component at 852.7 eV, which is characteristic of Ni^0, and a minor bump at 857.2 eV, which can be mixed Ni^{2+} components from $Ni(OH)_2$ and NiO. The significant reduction in the Ni^{2+}-related peak indicates that the passivation layer of Ni powder was largely removed during the low-current charging periods. The disappearance of the passivation layer on the Ni powder for the charged cells containing FeS additive is in good agreement with the battery performance, which showed a lower overpotential and the full charging capacity (refer to Fig. 1). These results imply that the FeS plays a critical role in the activation of a Na–$NiCl_2$ cell by removing the passivation layer of Ni particles, and hence allowing an electrochemical reaction (Ni redox) to occur on the surface of the Ni powder. To the best of our knowledge, this critical role of FeS in the Na–$NiCl_2$ battery has not been reported in detail elsewhere. Regarding the reaction of FeS, Sudworth proposed a possible electrochemical reaction of FeS as follows: [14]

$$FeS + 2NaCl + Ni \rightarrow FeCl_2 + NiS + 2Na \quad E = 2.37\ V$$

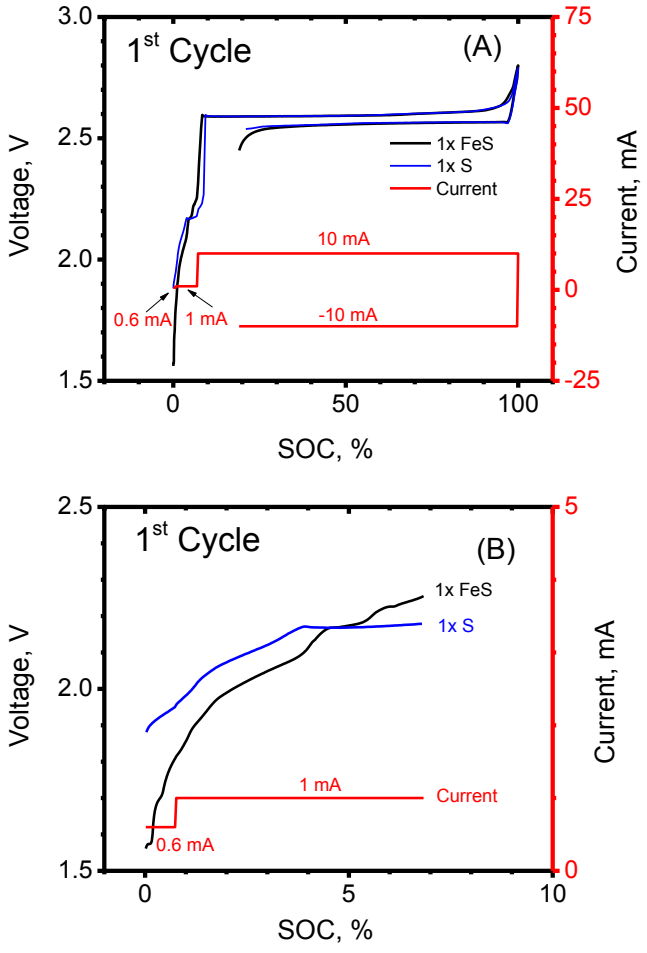

Fig. 3. Voltage profile (first cycle) for batteries with sulfur (1× loading, blue) and FeS (1× loading) for maiden charge and discharge (A), and expanded view of voltage profile for low-current charge period (B). (For interpretation of the references to color in this figure legend, the reader is referred to the web version of this article.)

However, the results of electrochemical tests and XPS analysis suggested different electrochemical reactions of FeS. No obvious peaks related to NiS were observed in XPS spectra (Fig. 2C and 2D). Furthermore, the electrochemical reactions of FeS related to the removal of the passivation layer occurring during low-current charging steps revealed the voltage range from 1.6 to 2.2 V, as shown in the expanded views of voltage profiles (Fig. 1B). This voltage profile is similar to sulfur redox reactions which have been extensively investigated in Na–S batteries. The oxidation of sulfur

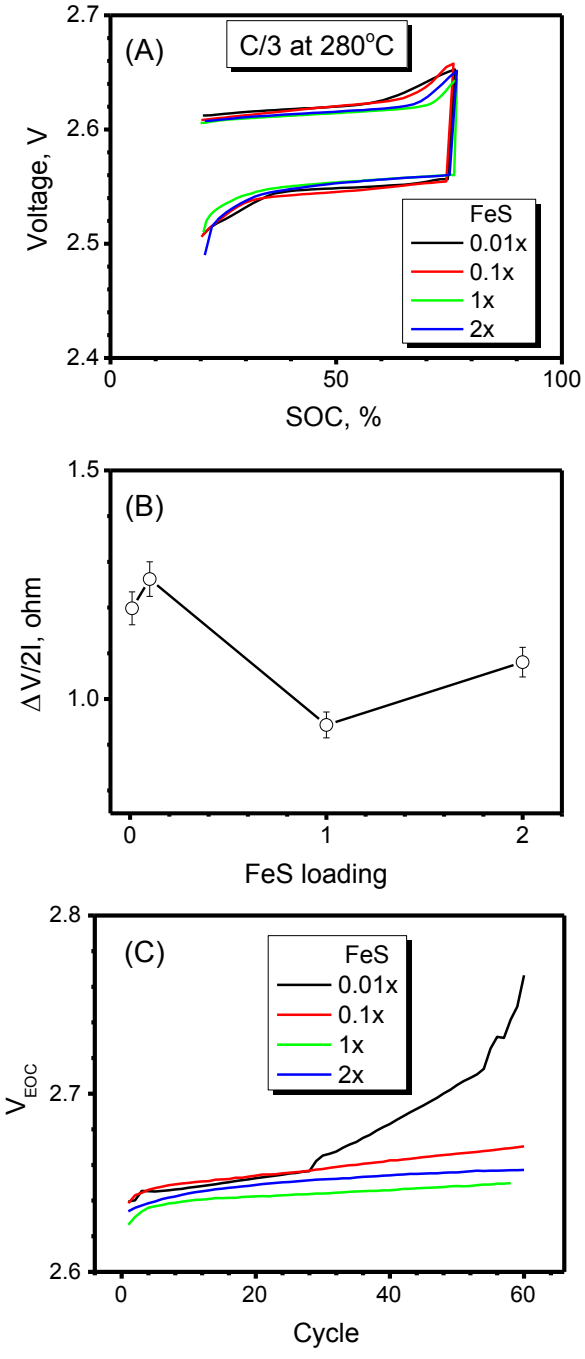

Fig. 4. (A) Voltage profiles (10th cycle) for C/3 (30 mA) tests for cells with FeS loading at 0.01× (black), 0.1× (red), 1× (green), and 2× (blue), respectively. (B) Resistance for different FeS loading cells at SOC 50% (10th cycle). See text for more detailed information. (C) End-of-charge voltage (EOC) plots of C/3 (30 mA) tests for each corresponding FeS loading over 60 cycles. (For interpretation of the references to color in this figure legend, the reader is referred to the web version of this article.)

during charging involves the formation of polysulfide species, such as S_n^{2-} ($n > 1$) [1]. The voltage profile related to the formation of polysulfide species in the Na–S battery ranges from 1.74 V ($Na_2S_{2.7}$) to 2.08 V (Na_2S_5) [1], which is close to the voltage profiles of the cell with 1× FeS during low-current charging steps. This indicates that polysulfide species were formed during low-current charging, rather than NiS, due to the reaction of FeS, NaCl and Ni. To test this hypothesis, a cell with 1× elemental sulfur instead of FeS was tested to eliminate the possibility of the reaction between FeS with NaCl and Ni. The cell with 1× sulfur shown in Fig. 3, which was expected to undergo polysulfide formation reaction, showed quite similar electrochemical behavior and voltage profile to those of the cell with 1× FeS. This result implies that FeS may have been decomposed to sulfur rather than directly reacted with NaCl and Ni, and the formation of elemental sulfur and polysulfide was related to the removal of a passivation layer on the Ni powder.

To evaluate the effects of FeS loadings on cell performance, cells with four different levels of FeS loadings (0.01×, 0.1×, 1×, and 2×) were tested at 280 °C at the C/3 rate (30 mA) with a fixed cycling capacity of 90 mAh (20~80% SOC). The cutoff voltages for charging and discharging were set at 2.8 V and 1.8 V, respectively. The typical voltage profiles for charging and discharging are shown in Fig. 4A. Due to the higher current density, the overpotentials of cells run at C/3 are generally higher than those run at lower currents shown in Fig. 1A. The cell with 1× FeS loading revealed the lowest overpotentials, especially at the end of charge. For a better comparison, the average polarization at 50% SOC was compared in Fig. 4B as defined by a following formula:

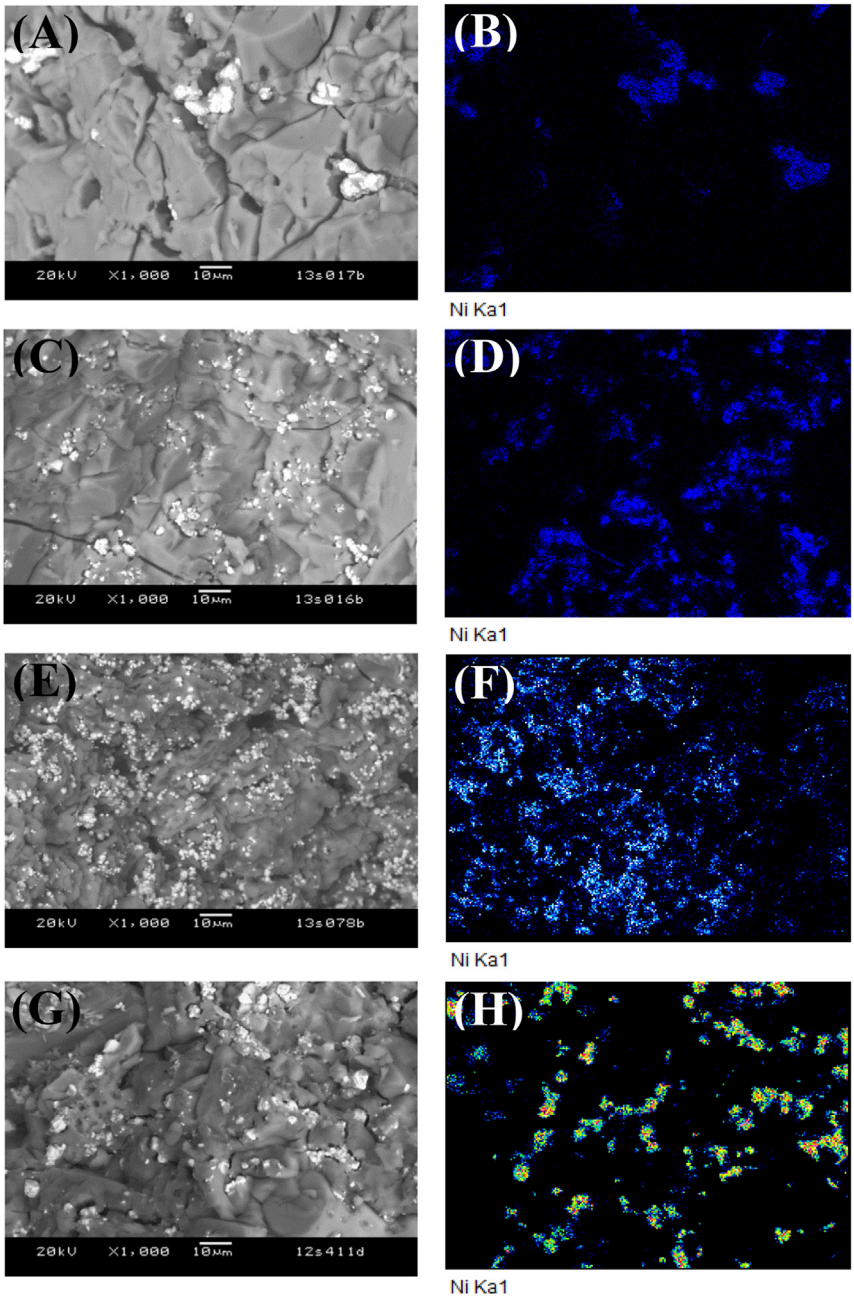

Fig. 5. (A), (C), (E), and (G): SEM images (backscattering, 1000×) for cathode granules from cells have different FeS loadings of 0.01×, 0.1×, 1×, and 2× after testing at C/3 for 60 cycles. (B), (D), (F), and (H): Ni mapping on corresponding SEM image shown on the left.

$P_{ave} = \Delta V/(2I) = (V_c - V_d)/(2I)$

where I is the current (30 mA), and V_c and V_d are voltages during charging and discharging at 50% SOC, respectively. The average polarization was higher (~1.25 ohm) for 0.01× and 0.1× FeS loadings, and decreased to 0.95 ohm for 1× FeS loading (~25% lower compared to 0.01× and 0.1× FeS). It is interesting that the average polarization increased again with further addition of FeS (2× FeS loading: ~14% higher compared to 1× FeS loading). This result is consistent with the trend of the voltage profile at the end of charging, where 1× FeS loading showed the least voltage rise (Fig. 4A). The degradation of each cell was observed in the change in the end-of-charge (EOC) voltage (Fig. 4C). As mentioned earlier, the EOC voltage (V_{EOC}) was initially lower for 1× FeS in comparison with 0.01×, 0.1×, and 2× FeS loadings. The cell with minimum FeS (0.01×) revealed the fastest degradation, as indicated by the rapid increase in V_{EOC} with cycles. For a more quantitative comparison, the voltage degradation rate (ΔV_{EOC}/cycle) was calculated by linear fitting of the slope of V_{EOC}–cycle plots between the 10th and 60th cycles, where the cells exhibited steady degradation. The ΔV_{EOC}/cycle values were 1.9 mV/cycle for 0.01× FeS, 0.41 mV/cycle for 0.1× FeS, 0.19 mV/cycle for 1× FeS, and 0.25 mV/cycle for 2× FeS. Thus, the cell with 1× FeS loading exhibited the slowest degradation rate as well as the lowest polarization.

The fracture surfaces of cathodes were observed using SEM after 60 cycles in order to understand the effects of microstructural change on cell degradation. Backscattered electron images and Ni mapping images collected from the cells with various FeS loadings are shown in Fig. 5. The brighter spots in the SEM micrographs represent Ni particles, as confirmed by EDS point analysis. It appears that the growth of Ni particles during cycles was influenced by the FeS loading level. The average particle size in the cell with 0.01× FeS loading is about 10 μm, which is almost an order of magnitude larger than the original size (particle size of raw Ni powder: 1–2 μm). In contrast, fine Ni particles close to the raw Ni powder were observed in the cell with 1× FeS loading, which also had the slowest degradation. The order of Ni growth (0.01X > 0.1X ≈ 2X > 1×) is consistent with that of the cell degradation rate (0.01X > 0.1X ≈ 2X > 1×).

It is important to understand the correlation between FeS loading and Ni particle growth, since Ni particle growth in cathodes is one of the important cell degradation mechanisms. It has been discussed by others and us that the larger Ni particles in the cathode lead to less active surface area for electrochemical reactions and poor electron percolation path [16,17]. Our previous publication [16] reported the correlations between battery operating conditions (such as C-rate, Ni/NaCl ratio, and SOC at the end of charge) and Ni particle growth. In summary, higher C-rate (high current density), lower Ni/NaCl ratio, and higher SOC at the end of charge (larger capacity window) tend to promote Ostwald ripening of $NiCl_2$, causing faster Ni particle growth. Although the initial amount of Ni powder was kept the same for all the cells with different FeS loadings, the amount of electrochemically active Ni can differ depending on the removal of the passivation layer. This deviation in electrochemically active Ni surfaces is most likely related to how much passivation layer has been removed by FeS. Incomplete removal of the passivation layer on the Ni particles possibly reduces the number of electrochemically active Ni particles, giving the same effect as a lower Ni/NaCl ratio. As reported in our previous work, [16] a low Ni/NaCl ratio and higher C-rate induces higher local current density on active Ni particles and consequently Ni particle growth. This is in good agreement with the experimental results, where the largest Ni particle size was observed on the cell with 0.01× FeS loading. It should be noted that the smallest size of Ni particle was observed for 1× FeS rather than 2× FeS; this indicates that excessive FeS also promotes the growth of Ni so that there is an optimum level of FeS loading which minimizes the Ni particle growth and the cell degradation.

4. Conclusions

In this work, we investigated the effects of FeS on cell activation and degradation of the Na–$NiCl_2$ battery. Detailed battery tests and XPS analysis revealed that FeS in the cathode plays a critical role in initial activation of batteries due to the removal of the surface passivation layer on Ni powders. The formation of polysulfide species rather than NiS was closely related to the removal of the passivation layer, which was observed in voltage profiles during cell activation and elemental sulfur addition. The removal of the surface passivation layers on Ni powder also influenced battery degradation. There is an optimum level of FeS that minimizes the particle growth of Ni and the degradation of cells since both incomplete removal and excessive FeS cause Ni particle growth. The operation and degradation mechanism of the Na–$NiCl_2$ battery have been conclusively addressed to understand the correlation between FeS in the cathode and Ni particle growth, which is critical for Na–$NiCl_2$ battery development for sustainable cycle lifetime, especially for large-scale energy storage applications.

Acknowledgments

This work was supported by the U.S. Department of Energy (DOE) Office of Electricity Delivery and Energy Reliability under Contract No. 57558. XPS characterizations were performed in the Environmental Molecular Sciences Laboratory, a national scientific user facility sponsored by DOE's Office of Biological and Environmental Research, located at Pacific Northwest National Laboratory (PNNL). PNNL is a multiprogram laboratory operated by Battelle Memorial Institute for the DOE under Contract DE-AC05-76RL01830.

References

[1] J.L. Sudworth, A.R. Tilley, The Sodium Sulfur Battery, Kluwer, New York, 1985.
[2] J.T. Kummer, N. Weber, Proc. SAE Congr. (1967) 1–6, 670179.
[3] Z.G. Yang, J.L. Zhang, M.C.W. Kintner-Meyer, X.C. Lu, D.W. Choi, J.P. Lemmon, J. Liu, Chem. Rev. 111 (2011) 3577–3613.
[4] B. Dunn, H. Kamath, J.M. Tarascon, Science 334 (2011) 928–935.
[5] K.B. Hueso, M. Armand, T. Rojo, Energ. Environ. Sci. 6 (2013) 734–749.
[6] C.H. Dustmann, J. Power Sources 127 (2004) 85–92.
[7] M.M. Thackeray, C. Wolverton, E.D. Isaacs, Energ. Environ. Sci. 5 (2012) 7854–7863.
[8] J.L. Sudworth, J. Power Sources 51 (1994) 105–114.
[9] R.C. Galloway, S. Haslam, J. Power Sources 80 (1999) 164–170.
[10] T. Tokunaga, A. Yoshida, A. Katagiri, Electrochemistry 73 (2005) 582–584.
[11] G.S. Li, X.C. Lu, C.A. Coyle, J.Y. Kim, J.P. Lemmon, V.L. Sprenkle, Z.G. Yang, J. Power Sources 220 (2012) 193–198.
[12] B.V. Ratnakumar, A.I. Attia, G. Halpert, J. Power Sources 36 (1991) 385–394.
[13] A. vanZyl, Solid State Ionics 86–88 (1996) 883–889.
[14] J.L. Sudworth, J. Power Sources 100 (2001) 149–163.
[15] X.C. Lu, J.P. Lemmon, V. Sprenkle, Z.G. Yang, JOM-US 62 (2010) 31–36.
[16] G.S. Li, X.C. Lu, J.Y. Kim, J.P. Lemmon, V.L. Sprenkle, J. Mater. Chem. A 1 (2013) 14935–14942.
[17] J. Prakash, L. Redey, D.R. Vissers, J. Electrochem. Soc. 147 (2000) 502–507.
[18] X.C. Lu, G.S. Li, J.Y. Kim, J.P. Lemmon, V. Sprenkle, Z.G. Yang, J. Power Sources 215 (2012) 288–295.
[19] C. Robelin, P. Chartrand, A.D. Pelton, J. Chem. Thermodyn. 36 (2004) 683–699.
[20] G. Parthasarathy, N. Weber, A.V. Virkar, ECS Trans. 6 (2007) 67–76.
[21] N.S. Mcintyre, M.G. Cook, Anal. Chem. 47 (1975) 2208–2213.
[22] T. Uchikoshi, Y. Sakka, M. Yoshitake, K. Yoshihara, Nanostruct. Mater. 4 (1994) 199–206.